

RESEARCH ARTICLE

10.1002/2014JD022846

Key Points:

- Satellite pixel-scale validation of a short-lived trace gas species
- Validation of TES satellite ammonia retrievals in an agricultural source region
- TES NH₃ columns at pixel scale reproduce in situ variability and column amounts

Correspondence to:

M. A. Zondlo,
mzondlo@princeton.edu

Citation:

Sun, K., et al. (2015), Validation of TES ammonia observations at the single pixel scale in the San Joaquin Valley during DISCOVER-AQ, *J. Geophys. Res. Atmos.*, 120, 5140–5154, doi:10.1002/2014JD022846.

Received 17 NOV 2014

Accepted 4 APR 2015

Accepted article online 9 APR 2015

Published online 22 MAY 2015

Validation of TES ammonia observations at the single pixel scale in the San Joaquin Valley during DISCOVER-AQ

Kang Sun^{1,2}, Karen Cady-Pereira³, David J. Miller^{1,2}, Lei Tao^{1,2}, Mark A. Zondlo^{1,2}, John B. Nowak⁴, J. A. Neuman⁵, Tomas Mikoviny^{6,7}, Markus Müller⁸, Armin Wisthaler^{6,7}, Amy J. Scarino⁹, and Chris A. Hostetler¹⁰

¹Department of Civil and Environmental Engineering, Princeton University, Princeton, New Jersey, USA, ²Center for Mid-Infrared Technologies for Health and the Environment, NSF-ERC, Princeton, New Jersey, USA, ³Atmospheric and Environmental Research, Lexington, Massachusetts, USA, ⁴Aerodyne Research, Inc., Billerica, Massachusetts, USA, ⁵Cooperative Institute for Research in Environmental Sciences, University of Colorado Boulder and NOAA Earth System Research Laboratory, Boulder, Colorado, USA, ⁶Institut für Ionenphysik und Angewandte Physik, Innsbruck, Austria, ⁷Department of Chemistry, University of Oslo, Oslo, Norway, ⁸Oak Ridge Associated Universities, Oak Ridge, Tennessee, USA, ⁹Science Systems and Applications Inc., Hampton, Virginia, USA, ¹⁰NASA Langley Research Center, Hampton, Virginia, USA

Abstract Ammonia measurements from a vehicle-based, mobile open-path sensor and those from aircraft were compared with Tropospheric Emission Spectrometer (TES) NH₃ columns at the pixel scale during the NASA Deriving Information on Surface conditions from Column and Vertically Resolved Observations Relevant to Air Quality field experiment. Spatial and temporal mismatches were reduced by having the mobile laboratory sample in the same areas as the TES footprints. To examine how large heterogeneities in the NH₃ surface mixing ratios may affect validation, a detailed spatial survey was performed within a single TES footprint around the overpass time. The TES total NH₃ column above a single footprint showed excellent agreement with the in situ total column constructed from surface measurements with a difference of 2% (within the combined measurement uncertainties). The comparison was then extended to a TES transect of nine footprints where aircraft data (5–80 ppbv) were available in a narrow spatiotemporal window (<10 km, <1 h). The TES total NH₃ columns above the nine footprints agreed to within 6% of the in situ total columns derived from the aircraft-based measurements. Finally, to examine how TES captures surface spatial gradients at the interpixel scale, ground-based, mobile measurements were performed directly underneath a TES transect, covering nine footprints within ±1.5 h of the overpass. The TES total columns were strongly correlated ($R^2 = 0.82$) with the median NH₃ mixing ratios measured at the surface. These results provide the first in situ validation of the TES total NH₃ column product, and the methodology is applicable to other satellite observations of short-lived species at the pixel scale.

1. Introduction

Ammonia (NH₃) is a key precursor to fine particulate matter and a critical component of the global nitrogen cycle. As the dominant alkaline atmospheric species, NH₃ reacts readily with atmospheric acidic species to form ammoniated aerosols, which have implications for human health [Paulot and Jacob, 2014], degrade regional air quality [Pinder et al., 2008], and influence the global radiation budgets [Shindell et al., 2009]. Deposition of NH₃ and ammoniated aerosols also contributes to substantial nitrogen loading in ecosystems downwind of intense NH₃ sources [Krupa, 2003]. Global sources and distributions of NH₃ are subject to considerable uncertainties [Clarisse et al., 2009; Sutton et al., 2013]. The magnitude and trends of emissions from different source types and source regions are even more uncertain [Reis et al., 2009; Clarisse et al., 2010]. Satellite and in situ observations consistently show higher values than model simulations, indicating significant underestimations of NH₃ emissions on multiple scales [Clarisse et al., 2009; Shephard et al., 2011; Heald et al., 2012; Nowak et al., 2012; Zhu et al., 2013; Schiferl et al., 2014; Van Damme et al., 2014a].

Measuring gas phase NH₃ at ambient levels, and at a spatiotemporal resolution relevant for validation of satellite NH₃ observations, has been challenging due to its partitioning between gas and particle phases, affinity for instrument sampling surfaces, and large spatiotemporal variations [von Bobrutski et al., 2010]. The atmospheric lifetime of NH₃ ranges from hours to days, depending on factors like deposition

processes and the presence of other reactive species [Baek and Aneja, 2004]; the global average atmospheric lifetime is about 11 h [Xu and Penner, 2012]. Therefore, NH_3 is highly concentrated in the planetary boundary layer (PBL) and NH_3 is concentrated near emission sources. Most of the current NH_3 measurement networks use passive samplers or dedicated denuders with a time resolution of days to weeks. For example, the U.S. Environmental Protection Agency monitors ambient NH_3 concentrations in the passive Ammonia Monitoring Network with a time resolution of 2 weeks. Aircraft [Nowak et al., 2010, 2012] and mobile [Sun et al., 2014] NH_3 measurements have been demonstrated to capture the spatial and temporal variations of NH_3 but only for the limited durations of measurement campaigns. The current scarcity of observations is of particular concern when considering the large spatiotemporal variability of NH_3 [Van Damme et al., 2015].

Satellite NH_3 observations complement current ground and airborne measurements by providing unique insights on NH_3 emissions and distributions from global to regional scales at semidaily to weekly frequencies. Global coverage of NH_3 has been obtained by the Tropospheric Emission Spectrometer (TES) instrument on the NASA Aura satellite [Shephard et al., 2011] and the Infrared Atmospheric Sounding Interferometer (IASI) instrument on the MetOp-A and MetOp-B satellite [Van Damme et al., 2014b]. NH_3 observations have been a standard TES product with global coverage since 2006. Because NH_3 is concentrated in the PBL, where infrared sounders typically have limited sensitivity [Boynard et al., 2014], successful retrieval of NH_3 is strongly dependent on the thermal contrast between the surface and lower atmosphere [Clarisse et al., 2010]. To most effectively use the vast number of satellite NH_3 observations, it is critical to validate them using in situ measurements under a wide range of atmospheric and surface conditions.

With that said, it is inherently challenging to use in situ measurements at a single location to validate polar-orbiting satellite measurements, which sample a large volume of air and rapidly pass over any given location on Earth. The horizontal spatial mismatch has been addressed by using statistical analyses over large satellite and in situ validation data sets [Boersma et al., 2009; Diao et al., 2013; Richter et al., 2014]. Spatial windows have been applied to include more satellite data at the expense of worsening the spatial mismatch for the intercomparison, and horizontal homogeneity is often assumed at the spatial window scale [Lamquin et al., 2012; Diao et al., 2013]. However, horizontal homogeneity is unlikely to be valid for NH_3 , which is characterized by a short lifetime and highly localized emission sources. Ground-based, vertically resolved measurements have been used to validate satellite columns of NO_2 [Chen et al., 2009], CO_2 [Morino et al., 2011], and CO [Sussmann and Buchwitz, 2005], but these techniques are not readily available for NH_3 . Overall, validating satellite NH_3 observations is additionally challenging due to its distribution in the atmosphere and lack of validation techniques.

Despite the availability and usage of satellite NH_3 observations from both TES and IASI, very few attempts of in situ validation have been reported so far. TES NH_3 representative volume mixing ratio (RVMR) data were compared with ground-based data from 25 sites in eastern North Carolina [Pinder et al., 2011]. The results showed that TES RVMR qualitatively captured the seasonal and spatial variabilities found in eastern North Carolina and overall had high correspondence with in situ data. However, the amount of quantitative information that could be drawn from this validation was limited by the spatial representativeness and temporal mismatch. Spatially, the ground sites used stationary, point sensors, whereas the TES RVMR represents an integrated abundance over a $5.3 \times 8.3 \text{ km}^2$ horizontal area at a certain height above a heterogeneous source region. Temporally, the ground-based measurements were averaged over 2 weeks, while the TES overpass was a snapshot at $\sim 13:30$ local time. The first validation of IASI NH_3 data by Van Damme et al. also indicated similar patterns between in situ measurements and satellite total NH_3 columns and highlighted the scarcity and limited spatiotemporal agreement of validation data sets [Van Damme et al., 2015].

In this study, TES NH_3 retrievals were validated in the San Joaquin Valley, California, at scales more closely resembling the TES footprint than Pinder et al. [2011] by using high-frequency vehicle- and aircraft-based measurements of NH_3 . Ammonia columns were constructed from vehicle- and aircraft-based measurements to compare with satellite observations. The validation environment of the San Joaquin Valley was challenging because NH_3 mixing ratios were highly heterogeneous within a single footprint due to numerous large emission sources. The spatial heterogeneity of NH_3 concentrations was characterized by a mobile laboratory sampling the satellite footprint within 1.5 h of the overpass time. The NH_3 vertical distribution was constrained from the NASA P-3B aircraft measurements during the NASA Deriving Information on Surface conditions from Column and Vertically Resolved Observations Relevant to Air Quality (DISCOVER-AQ) campaign [NASA, 2013]. The spatial coverage of the mobile laboratory enables

direct comparison between in situ and satellite measurements. We evaluate both how well the TES total column NH_3 data capture the pixel-scale variations at the surface level and the quantitative agreement with the in situ measurements. This approach has applications for the validation of the other NH_3 satellite observations and for validation of satellite measurements of other short-lived trace gas species.

2. Experimental Methods

The NASA DISCOVER-AQ campaign took place in the San Joaquin Valley of California on 16 January to 6 February 2013. During the campaign, the PBL height was low, and NH_3 mixing ratios within it were large. It was generally cloud free, and there was large thermal contrast (interquartile range of 6.6–10.7 K) at the TES overpass time during the day (around 13:30 local standard time, LST, same as all times mentioned in the following sections). Therefore, the meteorological conditions were ideal to test if the satellite could accurately see into the PBL.

2.1. Satellite Observations

TES is an interferometric spectral radiometer aboard the polar-orbiting Aura satellite, with 0.06 cm^{-1} unapodized spectral resolution and footprints of $5.3 \times 8.3 \text{ km}^2$ at nadir. The overpass time of TES is around 01:30 and 13:30 LST. The spectral and spatial resolutions of TES are considerably finer than most scanning infrared sounders, providing higher sensitivity in the PBL and allowing for the detection of more localized emission sources. TES has a number of observational modes (e.g., global survey, step and stare, and transect). The thermal infrared is measured in four spectral bands; the NH_3 retrieval uses a set of microwindows ranging from 962 to 969 cm^{-1} in the 1B2 band (923 – 1160 cm^{-1}). The radiometric noise lies between 0.1 K and 0.2 K at 950 cm^{-1} and 280 K [Clarisse *et al.*, 2010; Shephard *et al.*, 2011]. Current NH_3 retrievals generally have no more than one piece of vertical information (degree of freedom for signal (DOFS) < 1). A representative volume mixing ratio (RVMR), which is a weighted average of NH_3 mixing ratios over the region of the atmosphere where TES is sensitive, has been defined to relate column observations to tropospheric abundance [e.g., Shephard *et al.*, 2011]. An alternative way to present the one piece of vertical information is to use the total NH_3 columns, which is the approach by Van Damme *et al.* [2015] for IASI. The vertical NH_3 profiles from aircraft during the validation were characterized by high mixing ratios in the shallow PBL (400–800 m) with a rapid drop above the PBL. The free troposphere only contributed a small fraction of the total column. This vertical profile is very different from the TES a priori, which has a much slower decrease of mixing ratio above the PBL. Consequently, the altitude that the RVMR represents is significantly higher than the PBL top in most cases, whereas the actual NH_3 mixing ratio immediately above the PBL is 1–2 orders of magnitude lower than the mean PBL NH_3 mixing ratio. Therefore, we use the total NH_3 column product from TES version 6 data for direct comparison with in situ validation. During the NASA DISCOVER-AQ campaign in January 2013, TES made off-nadir transect observations with 20 footprints on the ground spaced 12 km apart along a line from Bakersfield to Fresno, California. The analyses were restricted to NH_3 retrievals with $\text{DOFS} \geq 0.5$ (75% of all retrievals used in this study). The average DOFS used in the analyses was 0.93 ± 0.10 , with a maximum of 1.10.

2.2. Mobile Measurements

Mobile NH_3 measurements were performed with an open-path, quantum cascade laser-based sensor mounted on the roof rack of a sedan passenger car [Miller *et al.*, 2014; Sun *et al.*, 2014]. The mobile laboratory also measured N_2O , CO [Tao *et al.*, 2012], CH_4 [McDermitt *et al.*, 2011], CO_2 , and H_2O (LI-7500, LICOR Biosciences Inc.) simultaneously. Meteorological parameters (temperature, pressure, relative humidity, wind direction, and wind speed) were measured on the vehicle with a portable weather station (Vaisala WXT520). Geolocation, vehicle speed, and driving direction were recorded with a GPS unit (GlobalSat EM-406a). Mixing ratios were measured at 5 Hz for trace gases and were averaged to 1 s and synchronized to the GPS time stamp. CO enhancements above background exceeding 500 ppbv were used as the criteria to remove measurements potentially contaminated by combustion-related NH_3 sources, including from our own or nearby vehicles. An in-line ethylene reference cell signal was probed continuously to account for sensor drift and provided real-time calibration to within $\pm 20\%$ accuracy for NH_3 [Sun *et al.*, 2013]. Off-line NH_3 calibration was also performed between field measurements based on the methods described in Miller *et al.* [2014] to achieve a final accuracy of $10\% \pm 0.2 \text{ ppbv}$ for 1 s data. The entire sensor platform operated on two 12 V

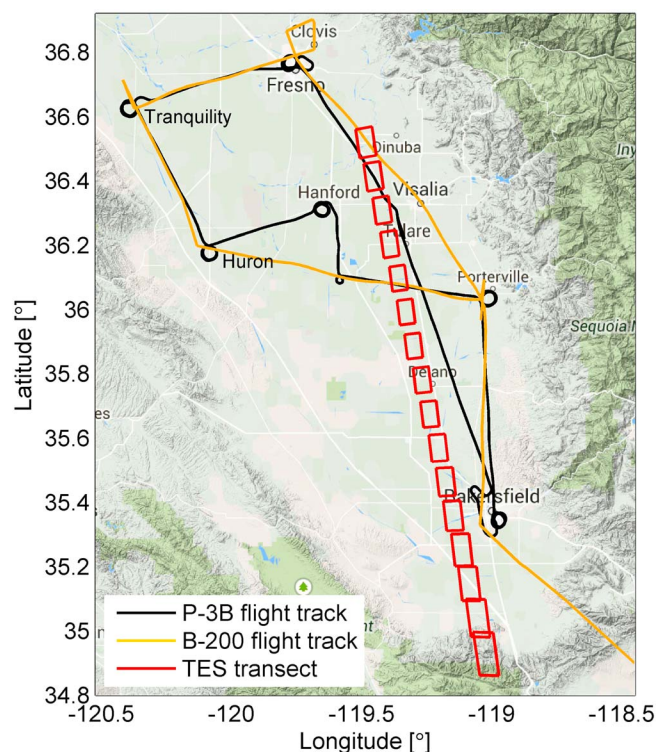


Figure 1. Map of the P-3B flight track (black line), B-200 flight track (orange line) in the San Joaquin Valley, and TES transect (red squares) on 30 January 2013. The vertical profiles were measured by the P-3B aircraft through spirals at the six sites labeled in the figure.

ground level (agl), and the ascent/descent rates were around 5 m s^{-1} . The diameter of spirals was about 5 km, slightly smaller than the TES footprint size.

NH_3 was measured simultaneously by a cavity ring down spectrometer (CRDS) and a proton-transfer-reaction time-of-flight mass spectrometer (PTR-ToF-MS) aboard the NASA P-3B aircraft. The CRDS (G2103, Picarro Inc.) reported NH_3 mixing ratios every approximately 3 s, with a total uncertainty of $\pm(35\% + 1.1 \text{ ppbv}) + 0.34 \text{ ppbv}$, where 0.34 ppbv is the 1σ precision. The CRDS sampling inlet configuration is very similar to that described in Nowak *et al.* [2010], though approximately 60 cm longer due to the installation constraints. The instrument background was determined periodically in-flight by overfilling the inlet with ambient air pushed through a scrubber filled with commercially available silicon phosphates (Perma Pure, Inc.). Standard addition calibrations were performed regularly with the output of a thermostated, flow-controlled, pressurized NH_3 permeation device (Kin-tek, La Marque, TX). The output of the NH_3 permeation device was quantified by UV absorption on the ground between each flight [Neuman *et al.*, 2003]. The response time was 8–20 s, defined as the 80% fall time of a 20 to 75 ppbv standard addition calibration. The PTR-ToF-MS [Müller *et al.*, 2014] had a measurement accuracy of $\pm 35\%$ and a 1σ measurement precision of 5.5–6.5 ppbv at 1 s time resolution. The response time was less than 7 s, which was determined as the risetime from instrumental zero to 100 ppbv ambient NH_3 concentration. The PTR-ToF-MS was calibrated on the ground by the same NH_3 permeation device used for CRDS. The field performances of the two sensors are compared in Figure 2, where two sets of aircraft spiral vertical profiles from 30 January 2013 are presented. The two vertical profile sites, Porterville and Hanford, were relatively close in space (65 km), and the time difference between the two spirals was only ~ 20 min. The aircraft made a spiral down from the free troposphere into the PBL at Porterville and a spiral up from the PBL into the free troposphere at Hanford. The PBL structures were similar at the two sites; the PBL heights, determined by the potential temperature profiles shown in Figure 2a, were about 600 m and 650 m agl at Porterville and Hanford, respectively. Figures 2b and 2c compare the NH_3 vertical profiles measured by the CRDS and PTR-ToF-MS at the two sites. The CRDS showed significantly better signal-to-noise ratio than the PTR-ToF-MS, whereas the hysteresis effects were

car batteries with a total run time on full charge of ~ 12 h. Exploiting the mobility of the sensing system, the spatial heterogeneity of NH_3 at the satellite footprint scale was characterized by driving along the satellite transect within 1 or 2 h of the overpass time.

2.3. Airborne Measurements

Airborne transects, vertical profiles, and ground-based measurements were conducted during 10 research flights in the San Joaquin Valley, California. Figure 1 shows flight circuits of the NASA P-3B and B-200 aircraft at 10:20–12:30 on 30 January 2013. TES transects for the same day are also displayed. The P-3B aircraft repeated a similar flight pattern on most of the flights during the campaign and usually performed three circuits per flight day. The B-200 aircraft generally followed the P-3B flight pattern. The P-3B aircraft performed spiral vertical profiles over six sites: Bakersfield, Porterville, Hanford, Huron, Tranquility, and Fresno. The altitude range for the vertical profiles

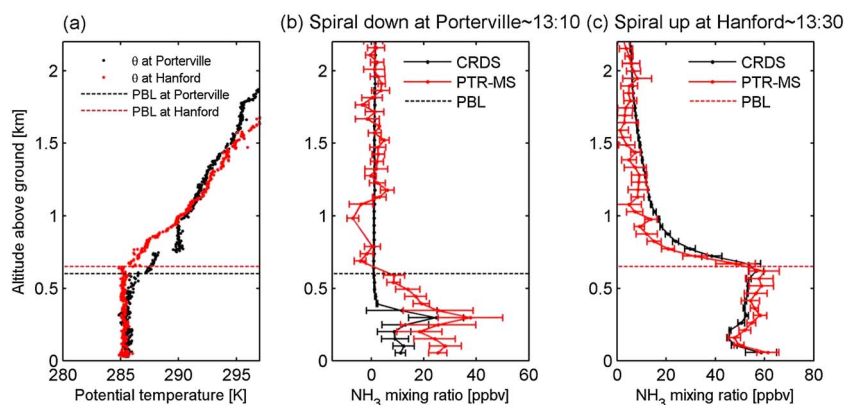


Figure 2. (a) Vertical profiles of potential temperature (θ) measured on the P-3B aircraft at Porterville and Hanford on 30 January 2013. (b) NH_3 vertical profiles measured by the CRDS (black) and the PTR-ToF-MS (red) during the downward spiral at Porterville. Data were vertically binned every 50 m, giving a temporal resolution of ~ 10 s, which is shorter than the response time of CRDS. Therefore, each CRDS data point may not be fully independent. The horizontal bars indicate 1σ variation within each bin. (c) Same as Figure 2b except with data during the upward spiral at Hanford.

more prominent for the CRDS when entering and exiting the PBL. Considering the advantages of both sensors, we investigate the vertical NH_3 structure in the PBL using the PTR-ToF-MS data and the free troposphere NH_3 concentration using the CRDS data.

Data from the NASA Langley Research Center airborne High Spectral Resolution Lidar (HSRL) onboard the B-200 aircraft were used for estimating mixed layer heights [Scarino *et al.*, 2014] in the study region. Aerosol mixing layer heights, which are a good proxy for PBL heights during the daytime, were derived by identifying sharp gradients in aerosol backscatter (532 nm) profiles. The aerosol backscatter values were averaged over ~ 1000 m horizontal and 30 m vertical resolution. The PBL heights were also validated thermodynamically using potential temperature vertical profiles measured during P-3B spirals (Figure 1), and the PBL heights determined thermodynamically agreed with HSRL PBL heights to within 10%.

2.4. Agricultural NH_3 Emission Plume Modeling

Animal farms, mainly dairy feedlots, account for 79% of the total NH_3 emissions in Tulare County [Environmental Protection Agency, 2013; California Department of Food and Agriculture, 2014], where the case studies of the TES transects took place. The average area of dairy farms in Tulare County is 0.22 km^2 [Department of Water Resources (DWR), 2007], much smaller than the TES footprint size of $\sim 40 \text{ km}^2$. The spatial scale of dairy farms is smaller than the resolutions of most chemical transport models and spatially allocated NH_3 emission inventories. To quantitatively simulate concentrations, one would need a large eddy simulation model to resolve turbulence, which is beyond the scope of this study. Instead, we used an area source Gaussian plume model [Smith, 1993] to qualitatively simulate the surface NH_3 abundance downwind of farm sources. Individual farm locations and shapes were obtained using the California Department of Water Resources land use data set for Tulare County in 2007 (386 dairy farms) [DWR, 2007]. Google Earth imagery from August 2012 was used to verify the locations manually and check for land use changes since 2007. In situ measured meteorological parameters (temperature and wind velocity) from the PBL transects of P-3B aircraft were incorporated in the plume model. The key assumptions of this area source Gaussian plume model are the following: (1) the emissions from the pasture/road/barren land surrounding the farms are negligible, (2) the wind and temperature field were stationary and homogeneous, (3) the depositional loss of NH_3 was insignificant at the spatiotemporal scales of interest, and (4) emissions per unit area were uniform across a farm. Therefore, modeled NH_3 abundance was used to demonstrate spatial heterogeneities rather than absolute mixing ratios.

2.5. Data Coverage

The analysis focuses on the TES transect observations on 21, 28, and 30 January 2013 in the San Joaquin Valley. Other TES transects during DISCOVER-AQ occurred on 23 January and 6 February but are not included in these analyses due to either a lack of mobile measurements or unsuccessful satellite retrievals (e.g., due to clouds).

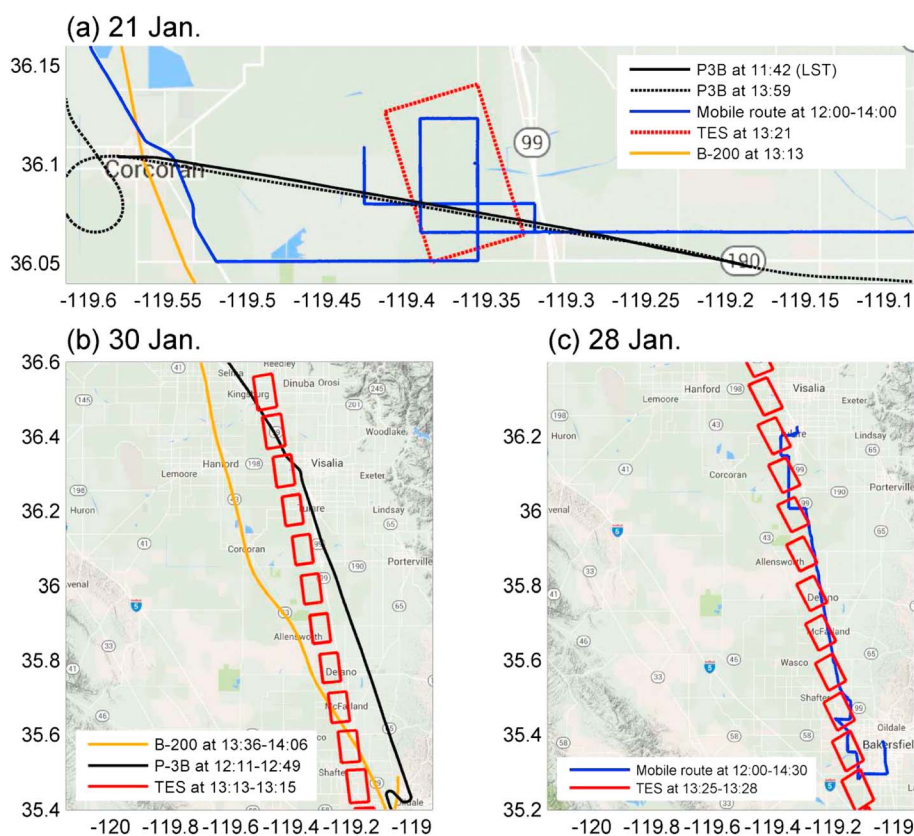


Figure 3. Overview of in situ airborne and ground-based mobile measurements used for TES validation. The measurement times (LST) are shown in the legends. (a) Single footprint spatial survey on 21 January 2013. (b) TES, P-3B, and B-200 transects on 30 January 2013. (c) TES transects and collocated mobile sampling route on 28 January 2013.

Figure 3 summarizes the in situ data sets that were used in this study to validate the TES total NH_3 column. The mobile laboratory made a detailed spatial survey within a single TES footprint on 21 January. The P-3B aircraft also made two transects in the PBL before and after the TES overpass. In addition, the B-200 aircraft flew by the TES footprint almost at the satellite overpass time (Figure 3a). The P-3B and B-200 aircraft flights were well aligned with the TES transect on 30 January (Figure 3b). Surface measurements along the TES transect were performed by the mobile laboratory on 28 January, when there were no research flights in the San Joaquin Valley (Figure 3c). The in situ measurements generally occurred within 1 h of the TES overpass time, as shown by the measurement time in Figure 3.

3. Results and Discussion

The type of validations on each of the three different TES overpass days varied due to spatiotemporal differences between the aircraft, mobile laboratory, and TES overpass and the availability of aircraft/mobile laboratories themselves. The total NH_3 column was constructed from mobile measurements on the ground and airborne measurements within a single TES footprint on 21 January 2013 and intercompared with the TES total column. Following a similar method, total NH_3 columns were constructed using airborne measurements collocated along a multipixel TES transect on 30 January 2013. Only ground-based, mobile measurements were used along a similar multipixel TES transect on 28 January 2013. Each of these case studies provided insight into the capabilities of TES to capture surface and boundary layer NH_3 spatial gradients as well as quantifying absolute agreement of between the ground-, aircraft-, and satellite-based NH_3 measurements.

3.1. Single Pixel Validation

A detailed spatial survey underneath a single TES footprint (36.0956°N , 119.3723°W) was performed on 21 January 2013 by the mobile laboratory. The TES overpass time was 13:21, and the mobile spatial survey

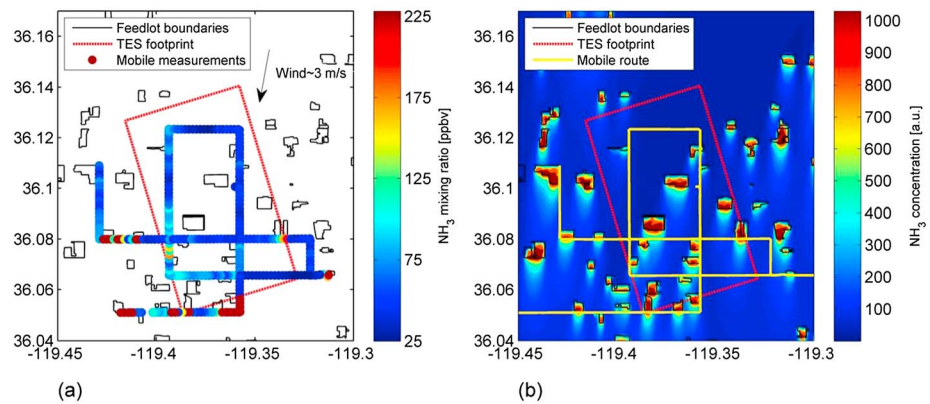


Figure 4. (a) Ground-based mobile NH_3 mixing ratio (ppbv) measurement near a TES footprint on 21 January 2013. Average wind direction and speed measured by the weather station are shown by the vector. (b) Gaussian dispersion plume simulation of the surface NH_3 concentration field over the sampling domain.

was conducted at 12:00–13:30. The P-3B aircraft made three transects in the PBL across the TES footprint at 9:22, 11:42, and 13:59. The latter two transects at flight altitudes of 296 ± 5 m (mean $\pm 1\sigma$ variation in the footprint) and 308 ± 6 m agl, respectively, were investigated due to their bracketing of the TES overpass time. The mobile sampling route and aircraft flight tracks are illustrated in Figure 3a. The PBL height was 451 ± 25 m, measured by the HSRL on the B-200 aircraft, which flew 18 km to the west of the TES footprint at 13:13. It is assumed that the PBL height measurements from B-200 aircraft were representative of the condition at the location of the TES footprints given the small spatiotemporal mismatch. Previous work in the Los Angeles basin also found that the HSRL PBL height showed good agreement with PBL height measured at ground sites up to 30 km away [Scarino *et al.*, 2014].

Ammonia at the near-surface level (1.5 m above ground, corresponding to the mobile sensor height) was simulated by the area source Gaussian plume model near the TES footprint. Figure 4a shows the mobile NH_3 measurements near the TES footprint, spatially averaged every 50 m along the driving route to eliminate high-frequency atmospheric turbulence perturbations. High NH_3 concentrations were observed directly downwind of most dairy farms, with qualitative correspondence with the Gaussian plume simulation. For the Gaussian plume modeling, the NH_3 flux rate was assumed to be constant over the dairy farm surface. The plume simulation shown in Figure 4b provides a qualitative view over the entire sampling domain and additional evidence of the strong intrapixel variations. Given the strong NH_3 spatial heterogeneity near sources, it would be very challenging to compare a single stationary site located inside the footprint boundary with the integrated satellite observation. A similar heterogeneity may have impacted the representativeness of stationary sites in the study of Pinder *et al.* [2011], which was also performed in an NH_3 source region with only one surface site inside each footprint. The spatial survey and plume modeling within the current study's single footprint demonstrate the value of making multiple surface samples within the TES footprint. This is especially critical in areas where there are numerous and strong emission sources.

The average NH_3 mixing ratios measured during the latter two P-3B aircraft PBL transects across the TES footprint were 51 ± 4 ppbv (mean $\pm 1\sigma$ variation in the footprint boundary, 11:42) and 55 ± 10 ppbv (13:59) for the CRDS. Mean NH_3 mixing ratios increased slightly between the two P-3B transects that were 99 min before and 38 min after the TES overpass, respectively. However, the temporal evolution of NH_3 was insignificant given the measured variances due to strong spatial heterogeneities. Because of the similarity between these transects, the closest P-3B transect across the TES footprint at 13:59 was used in the analysis. Figure 5a shows the high time resolution NH_3 measurements from both the CRDS and the PTR-ToF-MS during the 13:59 transect. Inside the TES footprint, the PTR-ToF-MS captured two significant plumes at a time scale of ~ 5 s and spatial scale of ~ 600 m, whereas the CRDS did not observe these plumes. The different response times of each instrument were one reason for the discrepancy as the plumes were evident by other tracers (e.g., CO_2). However, even with a slower time response, the CRDS instrument would be expected to show some response to NH_3 plume enhancements of 100 to 200 ppbv.

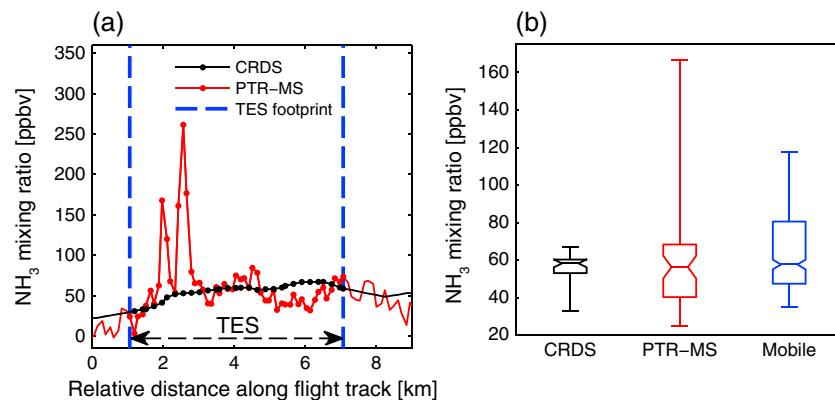


Figure 5. (a) Ammonia concentrations measured by CRDS (black) and PTR-ToF-MS (red) during the PBL transect across the TES footprint at ~13:59 on 21 January. Measurements made inside the footprint boundaries were highlighted. (b) Distributions of the airborne CRDS (black) and PTR-ToF-MS (red) NH_3 mixing ratio measurements and ground-based mobile measurements (blue) within the TES footprint boundary.

It is unclear why no response was observed here. Although the PTR-ToF-MS could detect high-frequency structures compared to the CRDS, the PTR-ToF-MS data showed extra variance due to larger random noise. The P-3B transects across the TES footprint lasted for ~60 s, much longer than the response times of both airborne sensors. Despite the occasional short-time scale differences between the two measurements, the median values within the TES footprint, 58 ppbv for the CRDS and 56 ppbv for the PTR-ToF-MS, were in excellent agreement. The distribution of the two airborne measurements during the 13:59 transect across the TES footprint is shown as a box-and-whisker plot in Figure 5b, together with the distribution of ground-based mobile measurements shown in Figure 4a. The surface measurements' distribution showed larger variance and was highly skewed toward higher concentrations due to enhancements measured at close proximity to the dairy farms. Despite the distinct distributions, the median of ground-based mobile measurements (57 ppbv) closely agreed with the median values of both airborne data sets.

In order to estimate a total NH_3 column using in situ data, it was necessary to assume a vertical profile of NH_3 . Although there were no collocated airborne vertical profile measurements within the TES footprints, it was possible to derive a representative vertical NH_3 profile using P-3B data at various spiral sites across the San Joaquin Valley. Figures 6a–6c show the spiral-up vertical profiles at Bakersfield, Hanford, and Tranquility averaged during the second and third circuits in the valley at 11:05–14:50. The PTR-ToF-MS data better represented the real vertical structure in the PBL by resolving the sharp gradient at the PBL top. The vertical profiles also indicate that NH_3 mixing ratios were much smaller (at least an order of magnitude) above the PBL compared to those within the PBL. The PBL-free troposphere NH_3 gradients were also clearly evident in the spiral-down profiles of the CRDS data (Figures 6d–6f). The mean free tropospheric NH_3 mixing ratio measured by the CRDS (up to the highest flight altitude of 2.5 km) was only 0.6 ± 0.6 ppbv at the three spiral-down sites during two circuits at 11:27–15:07. The free tropospheric NH_3 in DISCOVER-AQ was also consistent with aircraft measurements in the free troposphere during other field campaigns. For example, the mean NH_3 mixing ratio from 2.5 km to 6 km agl was 0.103 ppbv during Texas Air Quality Study campaign [Nowak *et al.*, 2010] and 0.185 ppbv during California Nexus campaign [Schiferl *et al.*, 2014]. Assuming a free troposphere mixing ratio of 0.6 ppbv up to 2.5 km, 0.2 ppbv from 2.5 km to 6 km, and 0 above 6 km, the free troposphere only contributes 3.6×10^{15} molecules cm^{-2} to the total column. For reference, the total column values observed by IASI in the San Joaquin Valley ranged from 10^{16} to 4.3×10^{17} molecules cm^{-2} [Van Damme *et al.*, 2014b]. Therefore, the free tropospheric contribution to the total column is expected to be small.

The excellent agreement between median surface and aircraft PBL measurements suggests that NH_3 was vertically uniform in the PBL at this single TES footprint. The vertical NH_3 profiles measured by the PTR-ToF-MS shown in Figures 2 and 6 imply that NH_3 was considerably well mixed in the PBL in these cases, although the large variability within an individual profile makes it difficult to assess their representativeness. To test this, normalized PBL NH_3 profiles were derived using the PTR-ToF-MS data during all flight days. The altitude of each vertical profile was normalized by the corresponding PBL height derived thermodynamically. NH_3

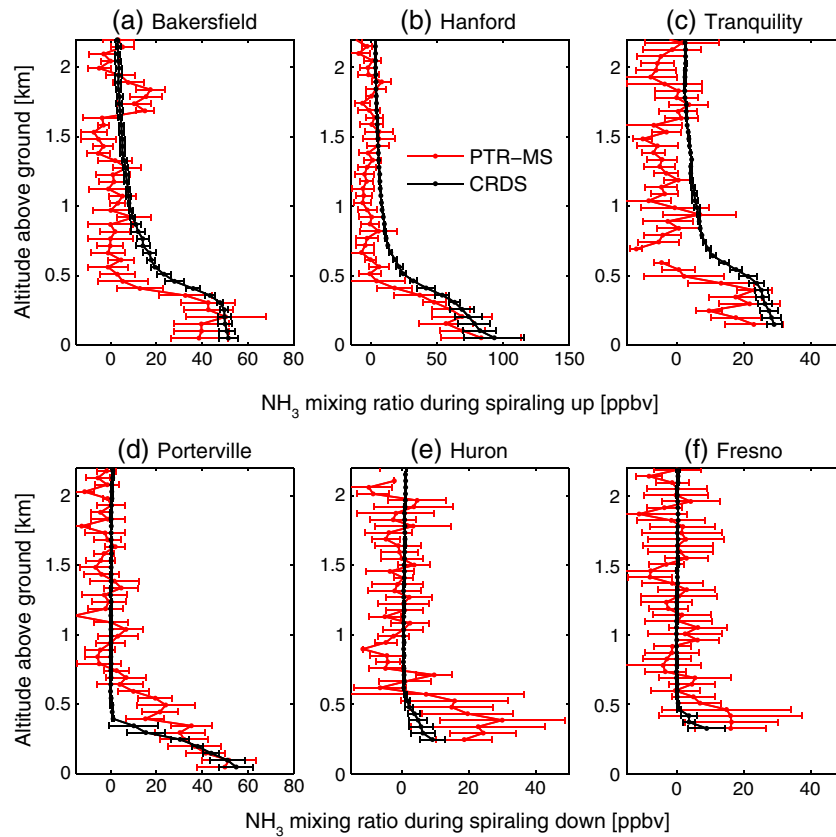


Figure 6. NH₃ vertical profiles during midday on 21 January measured by the CRDS (black) and the PTR-ToF-MS (red) during spiral up at (a) Bakersfield (35.33167, -118.99972), (b) Hanford (36.31572, -119.64323), and (c) Tranquility (36.63434, -120.38234) and during spiral down at (d) Porterville (36.03179, -119.05505), (e) Huron (36.19865, -120.10117), and (f) Fresno (36.78538, -119.77321). Data were vertically binned every 50 m. The horizontal bars indicate 1σ variation within each bin. Note that the instrumental uncertainties (~35%, see text) of both sensors are not shown.

mixing ratios were normalized by the mean mixing ratio in the PBL. Figure 7a summarizes all 76 vertical profiles measured between 11:50 and 14:50 LST (basically ±1.5 h from the TES overpass) during all flight days in the San Joaquin Valley. The normalized vertical profiles were binned into 10 intervals. Due to the large and skewed variations within each bin (the standard deviation was up to 100% of the mean), medians were used to construct a representative vertical profile. The median profile showed that NH₃ was well mixed in the lower 50% of the PBL and the normalized mixing ratio was lower near the top of the PBL due to entrainment of clean free tropospheric air. However, this median profile trend was much smaller compared to the variations within each vertical bin in which the interquartile ranges was up to 90% of the median value. The median profile including only vertical profiles on 21 and 30 January showed a very similar shape (Figure 7b). Although there is a recognizable trend in the median profile, the column abundance is only ~10% different from that of a perfectly uniform PBL profile. A representative PBL profile was estimated by interpolating the median profile of all vertical profiles shown in Figure 7a.

The in situ NH₃ column in the PBL was constructed using the surface median NH₃ mixing ratio (57 ppbv) and applying the representative PBL profile. The pressure profile was derived from the surface pressure measured by the mobile laboratory and the hydrostatic equation, and the temperature profile was derived using the P-3B measurement in the PBL assuming a dry adiabatic lapse rate. The in situ column within the PBL was 5.6×10^{16} molecules cm⁻² for the representative PBL profile derived from all airborne measurements. For reference, if one assumed a uniform PBL profile, the column abundance was 6.3×10^{16} molecules cm⁻². When adding the contribution from the free troposphere to the derived PBL column (3.6×10^{15} molecules cm⁻²), the agreement with the TES total column (5.9×10^{16} molecules cm⁻²) is excellent (2%) and well within the retrieval errors (±24%) and measurement uncertainties (±35%), as shown by Figure 8.

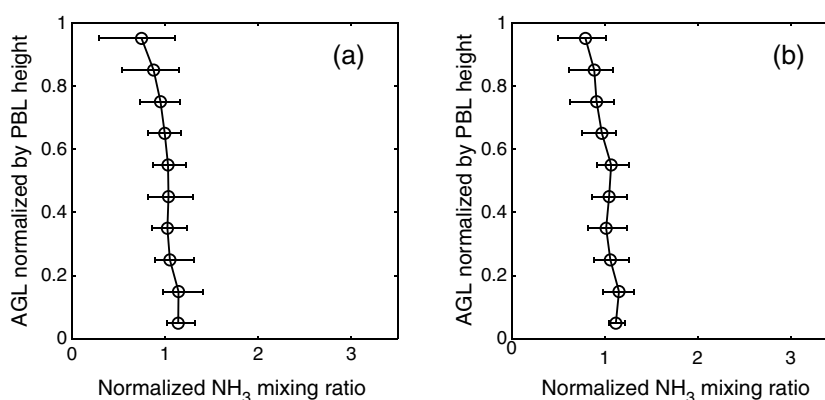


Figure 7. Median vertical NH_3 profile and interquartile range (25th to 75th percentiles of each bin) measured by the PTR-ToF-MS between 11:50 and 14:50 LST during (a) all flight days in DISCOVER-AQ and (b) only 21 and 30 January 2013.

3.2. Boundary Layer Aircraft Transect Validation

The total NH_3 column along a P-3B flight track on 30 January 2013 was thus constructed using the same method discussed in section 3.1. As shown in Figure 3b, the P-3B aircraft at 12:11–12:49 made a north-south transect that was well aligned spatially and in time with the TES transect at 13:13–13:15. The B-200 aircraft also made a north-south transect close to the TES transect at 13:36–14:06. Figure 9a shows the PBL height measured by the HSRL on the B-200 aircraft and the P-3B flight altitude above the ground. Figure 9b shows the NH_3 time series measured by the CRDS and PTR-ToF-MS on the P-3B. The two sensors showed excellent agreement during this measurement period, with a slope of 1.00 ± 0.01 and a R^2 of 0.90. Hence, the average values of the two sensors were used during this transect. Due to the differences in temporal resolution, the PTR-ToF-MS data were averaged to the time stamp of CRDS, and the two time series were averaged. The aircraft data were then binned according to the latitude boundaries of each TES footprint, and the medians in each bin were used to construct in situ total NH_3 columns at the corresponding TES footprint. The representative PBL profile derived previously was used to construct the total columns, although a uniform PBL profile yields differences less than 8%. The free tropospheric contributions were added as an uncertainty term of 3.6×10^{15} molecules cm^{-2} in the following analyses. Figure 9c compares the TES total columns with the in situ total columns. The total column data show close agreement within or close to the estimated TES error. The TES data captured the north-south NH_3 gradients in the PBL. The only significant discrepancy was at the southern end of the aircraft transect, where the P-3B flight track had the largest deviation from the TES transect (>10 km from the nearest TES footprint, as

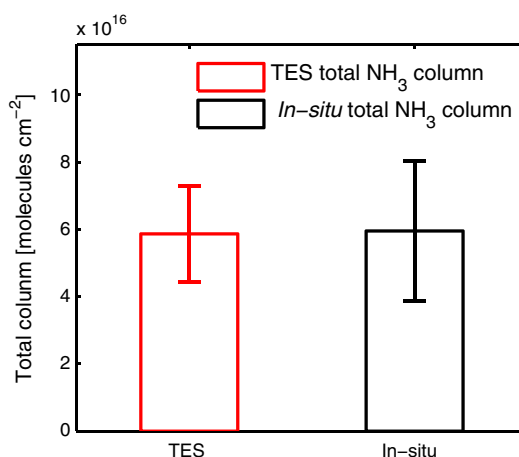


Figure 8. TES total NH_3 column (molecules cm^{-2}) at the single footprint on 21 January with retrieval error (red) and the constructed NH_3 column (molecules cm^{-2}) using in situ measurements.

shown in Figure 3b). Figure 9d shows the correlation between the total NH_3 columns constructed by in situ data and TES total NH_3 columns. Data points with spatial mismatch greater than 10 km were excluded. Total least squares regression shows good agreement between these two data sets (slope = 1.06, intercept = -3.9×10^{15} molecules cm^{-2} , $R^2 = 0.66$). Compared to the intrapixel variations and retrieval errors, shown as horizontal and vertical bars in Figure 9d, the difference between the two data sets is statistically insignificant.

3.3. Surface Concentrations Compared With Total Columns

Because NH_3 was concentrated in the PBL and the PBL was considerably well mixed

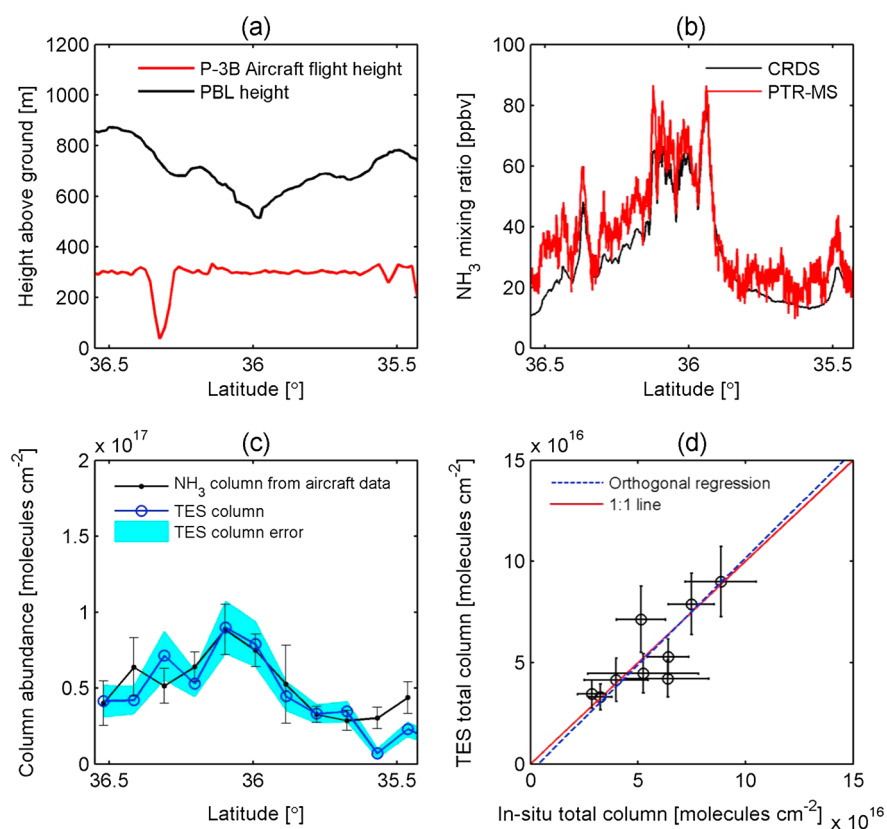


Figure 9. (a) PBL height (m) measured by the HSRL on the B-200 aircraft and the P-3B flight altitude above the ground on 30 January. The PBL height was smoothed by a 12 km window corresponding to the TES interpixel distance. (b) NH_3 mixing ratio (ppbv) measured by the CRDS (black) and PTR-ToF-MS (red). The two sensors show good agreement (slope = 1.00 ± 0.01 , intercept = 7.9 ± 0.4 ppbv, $R^2 = 0.90$). (c) TES total NH_3 column ($\text{molecules}/\text{cm}^2$) and the total column derived from the averaged aircraft data ($\text{molecules}/\text{cm}^2$). The error bars denote the standard deviation within each bin. (d) Correlation between the constructed total columns and TES total columns with total least squares (orthogonal) regression (slope = 1.06 ± 0.27 , intercept = $(-0.39 \pm 1.5) \times 10^{16}$ $\text{molecules}/\text{cm}^2$, $R^2 = 0.66$). The horizontal error bars denote the standard deviations of aircraft data within each bin. The vertical error bars denote the TES retrieval errors.

during these midday winter measurements, the ground-based mobile measurements would be expected to closely correlate with the satellite column measurements. While total columns could not be constructed from in situ measurements because there were no aircraft measurements in the San Joaquin Valley on 28 January, the satellite measurements could still be assessed by direct comparison to the surface measurements. Driving directly underneath TES transects at 12:00–14:30, nine footprints were covered by the mobile laboratory within ± 1.5 h of the TES overpass. Because one of these nine footprints had a DOFS < 0.5 , only eight footprints were used in the following analyses. The driving route was planned to minimize the spatial and temporal differences from TES transect. Off-highway measurements perpendicular to the TES track were performed to identify potential biases caused by vehicular NH_3 emissions on the highway. No significant differences between highway NH_3 mixing ratios and those upwind of the highway were found in the dairy region, suggesting that the on-road NH_3 contributions, when filtered by the CO measurements as described earlier, were small compared to farm emissions. The on-road NH_3 emission signals, although could be as high as hundreds of ppbv [Sun *et al.*, 2014], were easily distinguishable by their high variation frequencies and short durations. Simultaneous CO and CO_2 measurements on the mobile laboratory were also examined to identify vehicular emissions. Figure 10 shows the TES footprints, color coded by total NH_3 columns, and the mobile sampling route, color coded by NH_3 abundance from the surface measurements. The mobile data were spatially averaged every 1 km for better visualization. The dairy farm locations, taken from the California Department of Water Resources land use data set, are highlighted as polygons. Figure 11 shows the variation of surface NH_3 mixing ratios measured by the

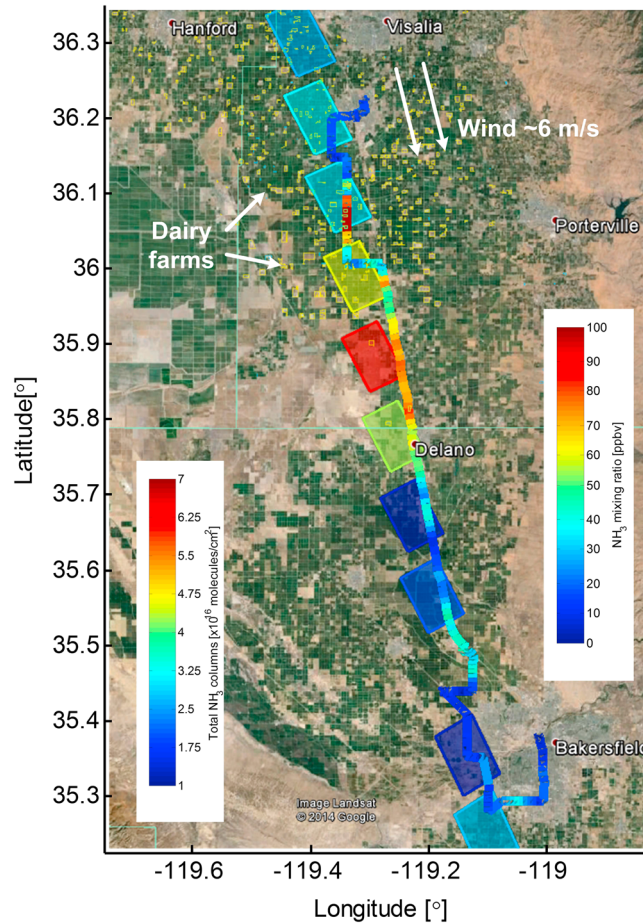


Figure 10. TES footprints on 28 January, color coded by the corresponding total NH_3 column values (molecules cm^{-2}), and mobile sampling routes, color coded by surface NH_3 mixing ratio. The dairy farms are highlighted as yellow polygons. The prevailing wind in the valley during the measurement period is illustrated.

mobile laboratory and the TES total columns. Both the ground-level mobile measurements and TES show elevated NH_3 values downwind the high dairy density region. The driving route was generally well downwind of the well-mixed emission plumes of many dairy farms with the exception of the TES footprint at 36.1°N , where the mobile measurements were strongly influenced by local individual farm

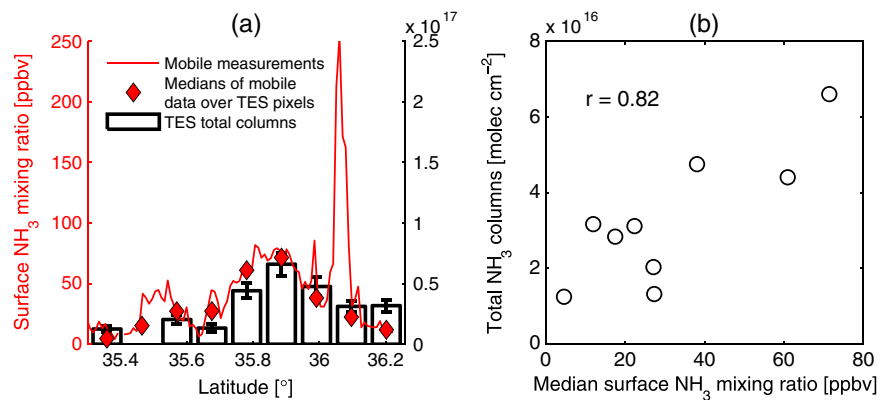


Figure 11. (a) Variation of surface NH_3 mixing ratio (ppbv) measured by the mobile laboratory and the TES total column (molecule cm^{-2}) on 28 January. (b) Correlation between median values of surface mixing ratio over TES footprints and TES total columns. The correlation coefficient is 0.82, which is statistically significant.

emissions and occasionally sampled extremely high concentrations (ppmv) directly downwind. However, the medians (red diamonds, Figure 11a) of mobile measurements over the TES footprints were not sensitive to the influences of individual local emissions. The spatial medians were more representative of the pixel than temporal means when extreme cases are frequently sampled. Similarly, Schiferl *et al.* [2014] used the medians of aircraft data in a grid box to compare with model concentrations from Goddard Earth Observation System chemistry model. The TES total columns were strongly correlated with these median values with a correlation coefficient of 0.82 (Figure 11b). This finding is consistent with the single footprint survey discussed in section 3.1, which showed that median values of a ground-based, mobile survey in a heterogeneous footprint are most likely to be representative of satellite field of view. This result of a ground-based mobile transect directly underneath the TES overpass indicates that TES total columns can also capture the surface NH₃ variations at the interpixel scale.

4. Conclusion

The total columns are considered to be the most fundamental satellite observation for atmospheric NH₃, given the limited vertical resolution. The total NH₃ column data from NASA TES/Aura instrument were validated by both aircraft- and vehicle-based in situ measurements during the DISCOVER-AQ campaign. In situ total columns were constructed using airborne or surface measurements and applying the representative PBL profile derived from airborne vertical profiles throughout the campaign. According to the airborne data, NH₃ in the PBL was considerably well mixed and dominated the total column abundance. The TES total NH₃ column above a single 5.3 × 8.3 km² footprint agrees with the in situ total column within 2%, which is less than the retrieval errors (±24%) and measurement uncertainties (±35%). NH₃ total column data from multiple TES pixels were compared with the total column constructed from airborne NH₃ mixing ratio during collocated aircraft sampling. The total column data show close agreement, and the aircraft values are within or close to the estimated TES error. In addition, data from another TES transect were compared with ground-based mobile measurements that covered a series of footprints. Both the ground-level mobile measurements and TES show elevated NH₃ values downwind of dairies with a significant correlation, suggesting that TES captured the surface NH₃ variability at interpixel scale. Overall, the TES total column data were accurate within the reported uncertainties in this validation environment.

Satellite NH₃ products have been used in many studies to evaluate model output and to constrain on NH₃ emission inventories, and there is an urgent need to validate these satellite NH₃ observations under a wide range of conditions. Compared with stationary sensors, mobile measurements achieve more flexible and representative spatial coverage without significant operational cost. Hence, the vehicle-based measurements provide more opportunities to compare surface level NH₃ with satellite total column values in more regions where the aircraft data are not available. The winter of the San Joaquin Valley provided this unique validation opportunity for its large NH₃ mixing ratios confined to a shallow PBL, large thermal contrast, and little contribution from NH₃ above the PBL. Additional validation is needed in different conditions, i.e., lower thermal contrast, lower PBL mixing ratios, or larger PBL heights.

The methodology demonstrated in this study is also applicable to other NH₃ satellite observations with comparable footprint size (e.g., IASI, Cross-track Infrared Sounder, and Atmospheric Infrared Sounder) and further to the validation of other short-lived species with sparse in situ observations. Satellites are often less sensitive to the PBL, where most of the short-lived species are concentrated. Acquiring surface NH₃ measurements at a stationary site that are representative of a satellite pixel average are challenging due to the strong spatial heterogeneity. However, a well-designed spatial survey should be able to capture local emission hot spots and obtain robust statistics to represent the footprint. Vertical profiles and PBL height measurements are of particular importance in linking in situ observations to satellite data.

References

- Baek, B. H., and V. P. Aneja (2004), Measurement and analysis of the relationship between ammonia, acid gases, and fine particles in eastern North Carolina, *J. Air Waste Manage. Assoc.*, 54(5), 623–633, doi:10.1080/10473289.2004.10470933.
- Boersma, K. F., D. J. Jacob, M. Trainic, Y. Rudich, I. DeSmedt, R. Dirksen, and H. J. Eskes (2009), Validation of urban NO₂ concentrations and their diurnal and seasonal variations observed from the SCIAMACHY and OMI sensors using in situ surface measurements in Israeli cities, *Atmos. Chem. Phys.*, 9(12), 3867–3879, doi:10.5194/acp-9-3867-2009.

Acknowledgments

We acknowledge the support of the NASA DISCOVER-AQ California 2013 science team, as well as Trent Proctor of the U.S. Forest Service for providing work and storage space in Porterville, California. We thank Michael Shook, Jennifer Olson, and Gao Chen for providing the merged airborne NH₃ data set and PBL heights derived from P-3B data and Robert Herman for providing the TES footprint coordinates before the overpass. The sensor development was supported by the Center for Mid-Infrared Technologies for Health and the Environment under National Science Foundation grant EEC-0540832. Kang Sun acknowledges support by NASA Earth and Space Science Fellowship (NN12AN64H). Work at AER was funded through a contract with the NASA Jet Propulsion Laboratory. The CRDS NH₃ measurements were made possible by the generous support from the DISCOVER-AQ program. NH₃ measurements by the PTR-ToF-MS aboard the NASA P-3B were supported by the Austrian Federal Ministry for Transport, Innovation and Technology (bmvit) through the Austrian Space Applications Programme 9 of the Austrian Research Promotion Agency (FFG) (840086). The measurement instrument was developed in joint work with Ionicon Analytik GmbH (Innsbruck, Austria). Armin Wisthaler received support from the Visiting Scientist Program at the National Institute of Aerospace. Tomas Mikoviny was supported by an appointment to the NASA Postdoctoral Program at the Langley Research Center, administered by Oak Ridge Associated Universities through a contract with NASA. The aircraft measurement teams acknowledge NASA B-200 King Air and P-3B flight crew for their outstanding work supporting these flights. All data used in this study are available at DISCOVER-AQ data archive (<http://www-air.larc.nasa.gov/cgi-bin/ArcView/discover-aq.ca-2013>).

- Boynard, A., et al. (2014), First simultaneous space measurements of atmospheric pollutants in the boundary layer from IASI: A case study in the North China Plain, *Geophys. Res. Lett.*, *41*, 645–651, doi:10.1002/2013GL058333.
- CDFA (2014), California Dairy Statistics 2013. [Available at http://www.cdfa.ca.gov/dairy/dairystats_annual.html.]
- Chen, D., B. Zhou, S. Beirle, L. M. Chen, and T. Wagner (2009), Tropospheric NO₂ column densities deduced from zenith-sky DOAS measurements in Shanghai, China, and their application to satellite validation, *Atmos. Chem. Phys.*, *9*(11), 3641–3662, doi:10.5194/acp-9-3641-2009.
- Clarisse, L., C. Clerbaux, F. Dentener, D. Hurtmans, and P. F. Coheur (2009), Global ammonia distribution derived from infrared satellite observations, *Nat. Geosci.*, *2*(7), 479–483, doi:10.1038/Ngeo551.
- Clarisse, L., M. W. Shephard, F. Dentener, D. Hurtmans, K. Cady-Pereira, F. Karagulian, M. Van Damme, C. Clerbaux, and P. F. Coheur (2010), Satellite monitoring of ammonia: A case study of the San Joaquin Valley, *J. Geophys. Res.*, *115*, D13302, doi:10.1029/2009JD013291.
- Diao, M., L. Jumbam, J. Sheffield, E. F. Wood, and M. A. Zondlo (2013), Validation of AIRS/AMSU-A water vapor and temperature data with in situ aircraft observations from the surface to UT/LS from 87°N–67°S, *J. Geophys. Res. Atmos.*, *118*, 6816–6836, doi:10.1002/jgrd.50483.
- Department of Water Resources (DWR) (2007), California Department of Water Resources Land Use Data. [Available at <http://www.water.ca.gov/landwateruse/lusvrymain.cfm>.]
- EPA (2013), The National Emission Inventory (NEI) 2011. [Available at <http://www.epa.gov/ttnchie1/net/2011inventory.html>.]
- Heald, C. L., et al. (2012), Atmospheric ammonia and particulate inorganic nitrogen over the United States, *Atmos. Chem. Phys.*, *12*(21), 10,295–10,312, doi:10.5194/acp-12-10295-2012.
- Krupa, S. V. (2003), Effects of atmospheric ammonia (NH₃) on terrestrial vegetation: A review, *Environ. Pollut.*, *124*(2), 179–221, doi:10.1016/S0269-7491(02)00434-7.
- Lamquin, N., C. J. Stubenrauch, K. Gierens, U. Burkhardt, and H. Smit (2012), A global climatology of upper-tropospheric ice supersaturation occurrence inferred from the Atmospheric Infrared Sounder calibrated by MOZAIC, *Atmos. Chem. Phys.*, *12*(1), 381–405, doi:10.5194/acp-12-381-2012.
- McDermitt, D., G. Burba, L. Xu, T. Anderson, A. Komissarov, B. Riensche, J. Schedlbauer, G. Starr, D. Zona, and W. Oechel (2011), A new low-power, open-path instrument for measuring methane flux by eddy covariance, *Appl. Phys. B*, *102*(2), 391–405.
- Miller, D. J., K. Sun, L. Tao, M. A. Khan, and M. A. Zondlo (2014), Open-path, quantum cascade-laser-based sensor for high-resolution atmospheric ammonia measurements, *Atmos. Meas. Tech.*, *7*, 81–93, doi:10.5194/amt-7-81-2014.
- Morino, I., et al. (2011), Preliminary validation of column-averaged volume mixing ratios of carbon dioxide and methane retrieved from GOSAT short-wavelength infrared spectra, *Atmos. Meas. Tech.*, *4*(6), 1061–1076, doi:10.5194/amt-4-1061-2011.
- Müller, M., et al. (2014), A compact PTR-ToF-MS instrument for airborne measurements of volatile organic compounds at high spatio-temporal resolution, *Atmos. Meas. Tech.*, *7*, 3763–3772, doi:10.5194/amt-7-3763-2014.
- NASA (2013), DISCOVER-AQ. [Available at http://www.nasa.gov/mission_pages/discover-aq/#.VFz4gfnF-K.]
- Neuman, J. A., T. B. Ryerson, L. G. Huey, R. Jakoubek, J. B. Nowak, C. Simons, and F. C. Fehsenfeld (2003), Calibration and evaluation of nitric acid and ammonia permeation tubes by UV optical absorption, *Environ. Sci. Technol.*, *37*(13), 2975–2981.
- Nowak, J. B., J. A. Neuman, R. Bahreini, C. A. Brock, A. M. Middlebrook, A. G. Wollny, J. S. Holloway, J. Peischl, T. B. Ryerson, and F. C. Fehsenfeld (2010), Airborne observations of ammonia and ammonium nitrate formation over Houston, Texas, *J. Geophys. Res.*, *115*, D22304, doi:10.1029/2010JD014195.
- Nowak, J. B., J. A. Neuman, R. Bahreini, A. M. Middlebrook, J. S. Holloway, S. A. McKeen, D. D. Parrish, T. B. Ryerson, and M. Trainer (2012), Ammonia sources in the California South Coast Air Basin and their impact on ammonium nitrate formation, *Geophys. Res. Lett.*, *39*, L07804, doi:10.1029/2012GL051197.
- Paulot, F., and D. J. Jacob (2014), Hidden cost of U.S. agricultural exports: Particulate matter from ammonia emissions, *Environ. Sci. Technol.*, *48*(2), 903–908, doi:10.1021/es4034793.
- Pinder, R. W., A. B. Gilliland, and R. L. Dennis (2008), Environmental impact of atmospheric NH₃ emissions under present and future conditions in the eastern United States, *Geophys. Res. Lett.*, *35*, L12808, doi:10.1029/2008GL033732.
- Pinder, R. W., J. T. Walker, J. O. Bash, K. E. Cady-Pereira, D. K. Henze, M. Z. Luo, G. B. Osterman, and M. W. Shephard (2011), Quantifying spatial and seasonal variability in atmospheric ammonia with in situ and space-based observations, *Geophys. Res. Lett.*, *38*, L04802, doi:10.1029/2010GL046146.
- Reis, S., R. W. Pinder, M. Zhang, G. Lijie, and M. A. Sutton (2009), Reactive nitrogen in atmospheric emission inventories, *Atmos. Chem. Phys.*, *9*(19), 7657–7677, doi:10.5194/acp-9-7657-2009.
- Richter, A., M. Weber, J. P. Burrows, J.-C. Lambert, and A. van Gijsel (2014), Validation strategy for satellite observations of tropospheric reactive gases, *Ann. Geophys.*, *56*, doi:10.4401/ag-6335.
- Scarino, A. J., et al. (2014), Comparison of mixed layer heights from airborne high spectral resolution lidar, ground-based measurements, and the WRF-Chem model during CalNex and CARES, *Atmos. Chem. Phys.*, *14*(11), 5547–5560, doi:10.5194/acp-14-5547-2014.
- Schiferl, L. D., C. L. Heald, J. B. Nowak, J. S. Holloway, J. A. Neuman, R. Bahreini, I. B. Pollack, T. B. Ryerson, C. Wiedinmyer, and J. G. Murphy (2014), An investigation of ammonia and inorganic particulate matter in California during the CalNex campaign, *J. Geophys. Res. Atmos.*, *119*, 1883–1902, doi:10.1002/2013JD020765.
- Shephard, M. W., et al. (2011), TES ammonia retrieval strategy and global observations of the spatial and seasonal variability of ammonia, *Atmos. Chem. Phys.*, *11*(20), 10,743–10,763.
- Shindell, D. T., G. Faluvegi, D. M. Koch, G. A. Schmidt, N. Unger, and S. E. Bauer (2009), Improved attribution of climate forcing to emissions, *Science*, *326*(5953), 716–718, doi:10.1126/science.1174760.
- Smith, R. J. (1993), Dispersion of odours from ground level agricultural sources, *J. Agric. Eng. Res.*, *54*(3), 187–200, doi:10.1006/jaer.1993.1013.
- Sun, K., L. Tao, D. Miller, M. A. Khan, and M. Zondlo (2013), Inline multi-harmonic calibration method for open-path atmospheric ammonia measurements, *Appl. Phys. B*, *110*(2), 213–222, doi:10.1007/s00340-012-5231-2.
- Sun, K., L. Tao, D. J. Miller, M. A. Khan, and M. A. Zondlo (2014), On-road ammonia emissions characterized by mobile, open-path measurements, *Environ. Sci. Technol.*, *48*(7), 3943–3950, doi:10.1021/es4047704.
- Sussmann, R., and M. Buchwitz (2005), Initial validation of ENVISAT/SCIAMACHY columnar CO by FTIR profile retrievals at the Ground-Truthing Station Zugspitze, *Atmos. Chem. Phys.*, *5*(6), 1497–1503, doi:10.5194/acp-5-1497-2005.
- Sutton, M. A. et al. (2013), Towards a climate-dependent paradigm of ammonia emission and deposition, *Philos. Trans. R. Soc. London, Ser. B*, *368*, 20130166, doi:10.1098/rstb.2013.0166.
- Tao, L., K. Sun, M. A. Khan, D. J. Miller, and M. A. Zondlo (2012), Compact and portable open-path sensor for simultaneous measurements of atmospheric N₂O and CO using a quantum cascade laser, *Opt. Express*, *20*(27), 28,106–28,118.
- Van Damme, M., R. J. Wichink Kruit, M. Schaap, L. Clarisse, C. Clerbaux, P.-F. Coheur, E. Dammers, A. J. Dolman, and J. W. Erismann (2014a), Evaluating 4 years of atmospheric ammonia (NH₃) over Europe using IASI satellite observations and LOTOS-EUROS model results, *J. Geophys. Res. Atmos.*, *119*, 9549–9566, doi:10.1002/2014JD021911.

- Van Damme, M., L. Clarisse, C. L. Heald, D. Hurtmans, Y. Ngadi, C. Clerbaux, A. J. Dolman, J. W. Erisman, and P. F. Coheur (2014b), Global distributions, time series and error characterization of atmospheric ammonia (NH_3) from IASI satellite observations, *Atmos. Chem. Phys.*, *14*(6), 2905–2922, doi:10.5194/acp-14-2905-2014.
- Van Damme, M., et al. (2015), Towards validation of ammonia (NH_3) measurements from the IASI satellite, *Atmos. Meas. Tech.*, *8*(3), 1575–1591, doi:10.5194/amt-8-1575-2015.
- von Bobrotzki, K., et al. (2010), Field inter-comparison of eleven atmospheric ammonia measurement techniques, *Atmos. Meas. Tech.*, *3*(1), 91–112.
- Xu, L., and J. E. Penner (2012), Global simulations of nitrate and ammonium aerosols and their radiative effects, *Atmos. Chem. Phys.*, *12*(20), 9479–9504.
- Zhu, L., D. K. Henze, K. E. Cady-Pereira, M. W. Shephard, M. Luo, R. W. Pinder, J. O. Bash, and G. R. Jeong (2013), Constraining U.S. ammonia emissions using TES remote sensing observations and the GEOS-Chem adjoint model, *J. Geophys. Res. Atmos.*, *118*, 3355–3368, doi:10.1002/jgrd.50166.